

# Charge and magnetic ordering in two-orbital double-exchange model for manganites

G. Jackeli<sup>a,b</sup>, N.B. Perkins<sup>a</sup>, and N.M. Plakida<sup>a</sup>

<sup>a</sup>*Joint Institute for Nuclear Research, Dubna, Moscow region, 141980, Russia*

<sup>b</sup>*Institute of Physics, Georgian Academy of Sciences, Tbilisi, Georgia.*

Phase diagram of half-doped perovskite manganites is studied within the extended double-exchange model. To demonstrate the role of orbital degrees of freedom both one- and two-orbital models are examined. A rich phase diagram is obtained in the mean-filed theory at zero temperature as a function of  $J$  (antiferromagnetic (AFM) superexchange interaction) and  $V$  (intersite Coulomb repulsion). For the one-orbital model a charge-ordered (CO) state appears at any value of  $V$  with different types of magnetic order which changes with increasing  $J$  from ferromagnetic (F) to AFM ones of the types A, C and G. The orbital degeneracy results in appearance of a new CE-type spin order that is favorable due to opening of the “dimerization” gap at the Fermi surface. In addition, the CO state appears only for  $V > V_c$  for F and CE states while C-type AFM state disappears and A-type AFM state is observed only at small values of  $V$  as a charge disordered one. The relevance of our results to the experimental data are discussed.

PACS numbers: 75.25.+z, 75.30.Et, 75.30.Vn, 71.45.Lr

## I. INTRODUCTION

Since early fifties<sup>1</sup> the physics of manganites challenge our current understanding of transition-metal oxides, and define both theoretical and experimental research problem that involves charge, spin, lattice and orbital degrees of freedom. Recently in a modern systematic experimental studies a very rich phase diagram (see, for example, Ref. 2) depending on the doping concentration, temperature and pressure was obtained in the doped manganese oxides with perovskite structure  $R_{1-x}B_xMnO_3$  (where R is trivalent rare-earth and B is divalent alkaline ion, respectively). At different doping concentration a full variety of magnetically ordered states such as antiferromagnetic (AFM) insulator, ferromagnetic (FM) metal and charge ordered (CO) insulator were observed. Many efforts have been made by theoreticians to understand it based on various models and approaches. Historically, double exchange (DE) model<sup>3</sup> was the basic one. In this model  $t_{2g}$ -electrons are localized, whereas the  $e_g$ -electrons are mobile and use O  $p$ -orbitals as a bridge between Mn ions. The hopping of itinerant electrons together with a very strong on-site Hund’s coupling drives core spins to align parallel. Qualitatively DE model gave appropriate interpretation of the phase diagram at the doping range  $0.2 < x < 0.5$  where FM metallic behavior was observed.

One of the subtle aspects of the perovskite manganites is the charge ordered state observed in almost all such compounds at half-doping.<sup>4-7</sup> A direct evidence of the CO state in half-doped manganites has been provided by the electron diffraction for  $La_{0.5}Ca_{0.5}MnO_3$ .<sup>5</sup> Similar observations have also been reported for  $Pr_{0.5}Sr_{0.5}MnO_3$ <sup>6</sup> and in  $Nd_{0.5}Sr_{0.5}MnO_3$ .<sup>7</sup> CO state is characterized by an alternating  $Mn^{3+}$  and  $Mn^{4+}$  ions arrangement in  $x - y$  plane with the charge stacking in  $z$ -direction. In CO state these systems show an insulating behav-

ior with a very peculiar form of AFM spin ordering. The observed magnetic structure is a CE-type and consists of quasi one-dimensional ferromagnetic zig-zag chains coupled antiferromagnetically. In addition, these systems show  $d_{3x^2-r^2}/d_{3y^2-r^2}$  orbital ordering. Another noteworthy observations were done by studying  $Pr_{1-x}(Ca_{1-y}Sr_y)_xMnO_3$  crystals with controlled one-electron bandwidth. As already mentioned above at half-doping  $Pr_{0.5}Ca_{0.5}MnO_3$  has a CO CE-type insulating state. However, by substitution Ca with Sr leading to the increase of the carrier bandwidth, one induces the collapse of the CO insulating state, and the A-type metallic state with  $d_{x^2-y^2}$  orbital ordering is realized in  $Pr_{0.5}Sr_{0.5}MnO_3$ .<sup>8</sup> The coexistence of the A-type spin ordered and CE-type spin/charge ordered states has been detected in the bilayer  $LaSr_2Mn_2O_7$ <sup>9</sup> and three-dimensional  $Nd_{0.5}Sr_{0.5}MnO_3$ .<sup>7</sup> These results indicate the competition between the metallic A-type  $d_{x^2-y^2}$  orbital ordering and the insulating CE-type  $d_{3x^2-r^2}/d_{3y^2-r^2}$  orbital ordering at half-doping and demonstrate the importance of the magnetic, charge and orbital order coupling in these compounds.

In recent publications it was shown that the DE anisotropy resulted from the orbital degeneracy with the peculiar  $e_g$  transfer amplitudes is important and to be a key point in explaining the various types of AFM ordering.<sup>10,11</sup> Until now most of the theoretical studies of CO state were done in the framework of the one-orbital model ignoring the double degeneracy of  $e_g$  orbitals.<sup>12-14</sup> The detailed mean-filed analysis of phase diagram of one-orbital DE model in the presence of both on-site and inter-site Coulomb terms has been given in Ref. 15. It has been shown, that in the vicinity of half-doping the double-exchange gain of energy is considerably suppressed by the inter-site Coulomb interaction that favors charge-ordered state. Recently, the CO state within the two-orbital model has been investigated by the projec-

tion perturbation techniques combined with the coherent state formalism and by Monte Carlo simulations in Refs. 16 and 17, respectively. In Ref. 16 the origin of CO has been attributed to the effective particle-hole interaction and CO state with C-type of the spin ordering at  $x = 0.5$  has been obtained. The Authors of Ref. 17 have shown that the experimentally observed charge, spin, and orbital ordering could be stabilized due to Jahn-Teller phonons.

In the present paper we investigate the role of the orbital degeneracy in the CO state based on the two-orbital DE model including the intersite Coulomb interaction. We adopt the mean-field (MF) approximation to derive the ground state phase diagram in the two-orbital model, and compare it to that of the corresponding one-orbital model. We argue that the orbital degeneracy together with the peculiar  $e_g$  transfer amplitude has a drastic effect on the phase diagram and is important in obtaining the realistic magnetic/charge/orbital ordering observed in half-doped manganites. The paper is organized as follows: In the next section the model Hamiltonian is presented and the mean-field scheme is formulated. The ground state phase diagrams of the one- and two-orbital models are derived and compared in Sec.III. Sec.IV summarizes our main results. In the Appendix the canonical transformation diagonalizing the MF Hamiltonian and the resulted band structure of various magnetic phases are presented.

## II. MODEL AND FORMULATION

We start with the two orbital ferromagnetic Kondo lattice model supplemented by the intersite Coulomb repulsion

$$H = - \sum_{\langle ij \rangle, \sigma} t_{ij}^{\alpha\beta} \left[ d_{i\sigma\alpha}^\dagger d_{j\sigma\beta} + H.c. \right] - J_H \sum_i \mathbf{S}_i \sigma_i + J \sum_{\langle ij \rangle} \mathbf{S}_i \mathbf{S}_j + V \sum_{\langle ij \rangle} n_i n_j - \mu \sum_i n_i. \quad (1)$$

The first term of Eq.(1) describes an electron hopping between the two  $e_g$  orbitals of the nearest neighbor (NN) Mn-ions. The orbitals  $d_{3z^2-r^2}$  and  $d_{x^2-y^2}$  correspond to  $\alpha(\beta) = 1$  and 2, respectively. Due to the shape of the  $e_g$  orbitals, their hybridization is different in the three cubic directions that leads to direction dependent hopping with the anisotropic transfer matrix elements  $t_{ij}^{\alpha\beta}$  given by

$$t_{x/y}^{\alpha\beta} = t \begin{pmatrix} 1/4 & \mp\sqrt{3}/4 \\ \mp\sqrt{3}/4 & 3/4 \end{pmatrix}, \quad t_z^{\alpha\beta} = t \begin{pmatrix} 1 & 0 \\ 0 & 0 \end{pmatrix}. \quad (2)$$

The second term in Eq.(1) describes the Hund's coupling between the spins of localized  $t_{2g}$ - electrons  $\mathbf{S}_i$  and the itinerant  $e_g$  electrons with spin  $\sigma_i$ . The superexchange (SE) interaction of localized spins between the NN sites

is given by  $J$ ,  $V$  represents the inter-site Coulomb repulsion of  $e_g$  electrons,  $n_i$  is the particle number operator and  $\mu$  is the chemical potential. The effect of the on-site Coulomb interaction that is not included in our model Hamiltonian will be discussed later.

We study the Hamiltonian (1) within the MF approximation, which is set up by introducing the order parameter for static charge-density wave of the form  $\langle n_i \rangle = n + \delta n \exp(i\mathbf{Q}\mathbf{R}_i)$ , with  $n$  being the electron density and  $\mathbf{Q} = (\pi, \pi, \pi)$ . Further, we treat localized spin subsystem classically and assume a strong Hund's coupling  $J_H \gg zt/S$ . In this limit one may take the local spin quantization axis parallel to  $t_{2g}$ -spins and in the rotated bases retain only "spin-up" components of the mobile electrons. Then the transfer integral between the NN sites is modified through relative angle of the  $t_{2g}$ -spins at the  $i$  and  $j$  sites as  $\tilde{t}_{ij}^{\alpha\beta} = t_{ij}^{\alpha\beta} \cos(\theta_{ij}/2)$ , where  $\theta_{ij}$  is the relative angle of the  $t_{2g}$ -spins. We consider the following magnetic phases that competes: i) Ferromagnetic configuration (F-type spin ordering) with  $\theta_{xy} = \theta_z = 0$  ( $\theta_{xy}$  and  $\theta_z$  are the angels between the neighboring spin in  $xy$ -plane and  $z$ -direction, respectively, ii) Layer-type antiferromagnetic configuration (A-type spin ordering) – the local spins are parallel in the planes and antiferromagnetically aligned between the neighboring planes, that corresponds to  $\theta_{xy} = 0$  and  $\theta_z = \pi$ . iii) Chain-type antiferromagnetic configuration (C-type spin ordering) – the local spins are parallel in the straight chains and antiferromagnetically coupled between the chains –  $\theta_{xy} = \pi$  and  $\theta_z = 0$ . iv) Neel-type antiferromagnetic configuration (G-type spin ordering) with all spins being antiparallel –  $\theta_{xy} = \theta_z = \pi$ . v) CE-type spin ordering with zig-zag ferromagnetic chains coupled antiferromagnetically.

As a result we come to the following MF Hamiltonian:

$$H = - \sum_{\langle ij \rangle, \alpha, \beta} \tilde{t}_{ij}^{\alpha\beta} \left[ d_{i\alpha}^\dagger d_{j\beta} + H.c. \right] - \Delta \sum_i e^{i\mathbf{Q}\mathbf{R}_i} n_i - \mu \sum_i n_i + 2(d-3)JS^2N, \quad (3)$$

where  $\Delta = zV\delta n$ ,  $z = 6$  for 3-dimensional cubic lattice, and  $d$  is dimensionality of the magnetic order ( $d = 0, 1, 2$ , and 3, respectively for G-, C-, A-, and F- type spin ordering). In Eq.(3) the zero of the energy is chosen in such a manner that the SE energy vanishes in the FM state. To obtain phase diagram we need to compare the free energies of all possible magnetic configurations.

## III. PHASE DIAGRAM

### A. One-orbital model

In order to incorporate the role of orbital degeneracy, first we consider the one orbital model ignoring the double degeneracy of  $e_g$  orbitals. Retaining only the one orbital per Mn-ion and assuming the isotropic transfer

amplitude, the electronic part of the MF Hamiltonian in  $\mathbf{k}$ -space is written as:

$$H_{\text{el}}^{\text{1orb}} = - \sum_{\mathbf{k}} (\tilde{t}_{\mathbf{k}} + \mu) d_{\mathbf{k}}^{\dagger} d_{\mathbf{k}} - \Delta \sum_{\mathbf{k}} d_{\mathbf{k}}^{\dagger} d_{\mathbf{k}+\mathbf{Q}}, \quad (4)$$

with

$$\tilde{t}_{\mathbf{k}} = 2t \sum_{i=1}^d \cos \mathbf{k}_i, \quad (k_1, k_2, k_3) = (k_x, k_y, k_z). \quad (5)$$

The above Hamiltonian (4) is easily diagonalized by the following canonical transformation:

$$d_{\mathbf{k}} = u_{\mathbf{k}} c_{1,\mathbf{k}} + v_{\mathbf{k}} c_{2,\mathbf{k}}, \quad d_{\mathbf{k}+\mathbf{Q}} = -v_{\mathbf{k}} c_{1,\mathbf{k}} + u_{\mathbf{k}} c_{2,\mathbf{k}} \quad (6)$$

with

$$u_{\mathbf{k}} = \frac{1}{\sqrt{2}} \left[ 1 - \frac{\tilde{t}_{\mathbf{k}}}{\varepsilon_{\mathbf{k}}} \right]^{\frac{1}{2}}, \quad v_{\mathbf{k}} = \frac{1}{\sqrt{2}} \left[ 1 + \frac{\tilde{t}_{\mathbf{k}}}{\varepsilon_{\mathbf{k}}} \right]^{\frac{1}{2}},$$

$$\varepsilon_{\mathbf{k}} = \sqrt{\tilde{t}_{\mathbf{k}}^2 + \Delta^2}. \quad (7)$$

In terms of the  $c$ -operators, the one particle Hamiltonian reads

$$H = \sum_{\mathbf{k},\alpha} (-1)^{\alpha} \varepsilon(\mathbf{k}) c_{\mathbf{k},\alpha}^{\dagger} c_{\mathbf{k},\alpha}, \quad \alpha = 1, 2. \quad (8)$$

At half-filling the chemical potential lies inside the gap ( $\mu = 0$ ) and recalling that  $\Delta = zV\delta n$  we receive a self-consistent equation for the order parameter

$$1 = \frac{zV}{2N} \sum_{\mathbf{k}} \frac{\tanh \beta \varepsilon_{\mathbf{k}}/2}{\varepsilon_{\mathbf{k}}}. \quad (9)$$

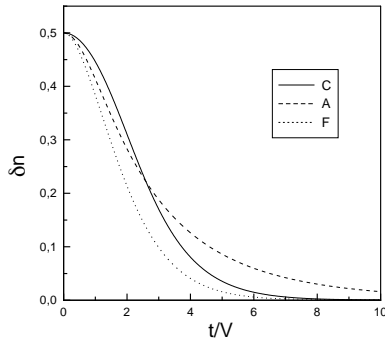


FIG. 1. The zero temperature charge order parameter  $\delta n$  as a function of  $t/V$  for the one-orbital model and for a different (F-, A-, and C-type) spin ordered states. Here  $t$  is the hopping amplitude and  $V$  is the intersite Coulomb repulsion.

In Fig.1 the overall behavior of the order parameter  $\delta n$  as a function of  $t/V$  is presented for various magnetic configuration. Since the wave vector summation in the right hand side of Eq.(9) diverges in the limit  $\Delta \rightarrow 0$  there exist a nontrivial solution even at  $V \rightarrow 0$  and hence a transition from homogeneous to CO state is continuous. We also note that  $\delta n$  diminishes exponentially with increasing the bandwidth (see Fig.1) indicating that the transition between the homogeneous and the CO state is a result of the competition between the kinetic and the electrostatic energy.

By comparing the free energies of different magnetic configuration we obtain the phase diagram as shown in Fig.2. At small  $V$ , with increasing  $J$  the system, starting from the F-CO phase, first enters to the C-CO phase and then to the G-CO state. Since the gain in the magnetic energy when the system moves from A- to C-phase is larger than the gain in the kinetic energy in C to A transition the A-CO phase is absent in this part of Phase diagram. With increasing of  $V$  at  $V \simeq 0.5t$  the CO gap in C-CO phase overcomes that one in A-CO phase that results in opening of small window of A-CO phase in the phase diagram. We also note that with increasing of  $V$  the SE coupling needed to stabilize the AFM configuration decreases since the bandwidth effect is overshadowed when the gap becomes larger. The different magnetic structures in Fig.2 are separated by the first-order boundaries. There is a jump in the charge order parameter across the phase boundaries, since the value of order parameter  $\delta n$  depends on the effective bandwidth and hence on the underlying magnetic structure, as can be seen from Fig. 2.

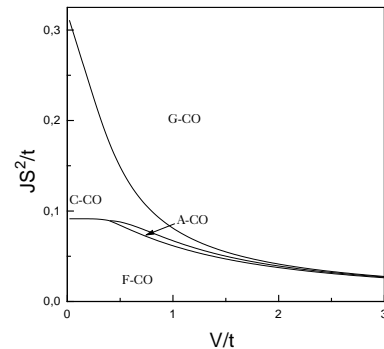


FIG. 2. Phase diagram of the one-orbital model in  $JS^2/t$  and  $V/t$  parameter plane. Here A, C, and G denotes the A-, C-, and G-type antiferromagnetic ordering, respectively, F denotes the ferromagnetic phase and CO is charge ordering. The solid lines stand for the first-order phase boundaries.

## B. Two orbital model

To describe the effect of orbital degeneracy, we consider the MF Hamiltonian (3) with anisotropic hopping

amplitude. In the momentum space the electronic part of the Hamiltonian reads as:

$$H_{\text{el}}^{2\text{orb}} = \sum_{\mathbf{k}, \alpha, \beta} [\varepsilon_{\mathbf{k}}^{\alpha\beta} - \mu\delta_{\alpha\beta}] d_{\mathbf{k}\alpha}^\dagger d_{\mathbf{k}\beta} - \Delta \sum_{\mathbf{k}, \alpha} d_{\mathbf{k}, \alpha}^\dagger d_{\mathbf{k}+\mathbf{Q}, \alpha} \quad (10)$$

with

$$\begin{aligned} \varepsilon_{\mathbf{k}}^{11} &= -\frac{1}{2}\tilde{t}_{xy}(\cos \mathbf{k}_x + \cos \mathbf{k}_y) - 2\tilde{t}_z \cos \mathbf{k}_z, \\ \varepsilon_{\mathbf{k}}^{12} &= \varepsilon_{\mathbf{k}}^{21} = -\frac{\sqrt{3}}{2}\tilde{t}_{xy}(\cos \mathbf{k}_x - \cos \mathbf{k}_y), \\ \varepsilon_{\mathbf{k}}^{22} &= -\frac{3}{2}\tilde{t}_{xy}(\cos k_x + \cos k_y) \end{aligned} \quad (11)$$

and  $\tilde{t}_{xy} = t \cos \theta_{xy}$ ,  $\tilde{t}_z = t \cos \theta_z$ .

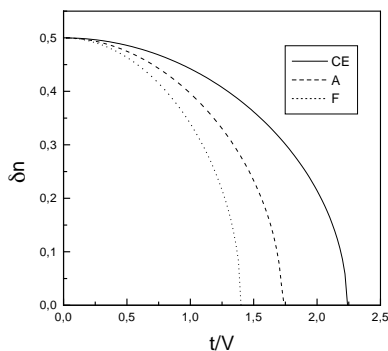


FIG. 3. Order parameter  $\delta n$  versus  $t/V$  for the two-orbital model and for a different (F-, A-, and CE-type) spin ordered states.

The diagonalization of this Hamiltonian ( see Appendix) leads to the four band model. In the case of F- and A-type spin ordering and at the filling corresponding to one electron per two Mn-ions (half-doped case) the gap is not opened at the Fermi surface, and the chemical potential moves down with the lower two bands. We solve the gap equation self-consistently with one for the chemical potential. As it seen in Fig.3, the transition to the charge ordered state is not continuous and there exists a critical value  $V_c$  above which the ordered state is favorable ( $V_c^F \simeq 0.72t$  and  $V_c^A \simeq 0.58t$  for F- and A-type spin ordering, respectively). As for the C-type spin

$$\begin{aligned} H_{\text{el}}^{\text{CE}} &= - \sum_{i, \alpha, \beta} \left\{ \left[ t_1^{\alpha\beta} \{ a_{i\alpha}^\dagger b_{i\beta} + \bar{a}_{i\alpha}^\dagger \bar{b}_{i\beta} \} + t_2^{\alpha\beta} \{ b_{i\alpha}^\dagger \bar{a}_{i\beta} + \bar{b}_{i\alpha}^\dagger a_{i+1\beta} \} + H.c. \right] \right. \\ &\quad \left. - (\mu + \Delta) \{ a_{i\alpha}^\dagger a_{i\alpha} + \bar{a}_{i\alpha}^\dagger \bar{a}_{i\alpha} \} - (\mu - \Delta) \{ b_{i\alpha}^\dagger b_{i\alpha} + \bar{b}_{i\alpha}^\dagger \bar{b}_{i\alpha} \} \right\} \end{aligned} \quad (13)$$

where  $i$  runs along the zig-zag and denotes the number of unit cell. Diagonalization of the above Hamiltonian ( see Appendix) leads to the complicated band structure consisting of bonding and antibonding bands,  $E_{a,b} = \pm \sqrt{\Delta^2 + t^2(2 - \cos(k/2))}$ , and nonbonding states  $E_{\pm} =$

ordering, there is no difference between the one and two orbital models in this sense. The existence of the additional orbital only introduce the localized level which is empty at the filling we consider.

The above Hamiltonian (10) describes the F-, A-, C-, and G-type spin ordering on an equal footing. However the presence of additional orbital degree of freedom, with the peculiar anisotropic transfer amplitudes  $t_{x,y,z}^{\alpha\beta}$  [see Eq.(2)] results in the anisotropic DE interaction<sup>18</sup> and may lead to the stabilization of CE spin ordering. Let us consider one zig-zag with two ferromagnetic bonds alternated in  $x$  and  $y$  directions (Fig.4). The corner and middle sites are denoted by  $a(\bar{a})$  and  $b(\bar{b})$ , respectively, and the unit cell is given by four nonequivalent atoms.

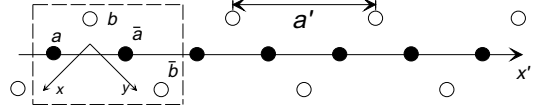


FIG. 4. The one isolated zig-zag shaped ferromagnetic chain. The real CE-type spin structure is given by this quasi-one-dimensional ferromagnets coupled antiferromagnetically. White and black circles denote  $\text{Mn}^{4+}$  and  $\text{Mn}^{3+}$  ions respectively. The dashed line shows the unit cell and  $a'$  is the lattice parameter along the zig-zag

For further discussions it is convenient to adopt the following bases of the  $e_g$  orbitals at nonequivalent sites:<sup>18</sup>  $|1\rangle = d_{3x^2-r^2}$ ,  $|2\rangle = d_{y^2-z^2}$ , and  $|\bar{1}\rangle = d_{3y^2-r^2}$   $|\bar{2}\rangle = d_{x^2-z^2}$  on  $a, b$  and  $\bar{a}, \bar{b}$  sites, respectively [see, Fig.4]. In the new bases the transfer matrix elements are given by

$$t_1^{\alpha\beta} = t \begin{pmatrix} 1 & 0 \\ 0 & 0 \end{pmatrix}, \quad t_2^{\alpha\beta} = t \begin{pmatrix} -1/2 & 0 \\ \sqrt{3}/2 & 0 \end{pmatrix} \quad (12)$$

between  $a-b$  ( $\bar{a}-\bar{b}$ ) and  $b-\bar{a}$  ( $\bar{b}-\bar{a}$ ) NN sites, respectively. As a result the zig-zag chain is modeled as a dimerized one with the alternating hopping amplitude and can be described by the following Hamiltonian

$\pm\Delta$ . Due to the topology of the zig-zag structure, only the directional  $d_{3x^2-r^2}$  ( $d_{3y^2-r^2}$ ) orbitals at  $a(\bar{a})$  sites give the input in the low energy bonding state [see Appendix for a details]. While for the  $b(\bar{b})$  sites both two orthogonal orbitals do contribute. Therefore, the orbital de-

generacy is removed on the middle site sublattice and the carriers on this sublattice will occupy the directional orbitals, leading to the polarized orbital state with  $d_{3x^2-r^2}/d_{3y^2-r^2}$  orbital ordering. We also emphasize, that at half-doping the bonding band is full and the system is a band insulator even in the absence of the charge ordering. The onset of the charge ordering renormalizes the gap to higher value. The behavior of the charge order parameter is depicted in Fig.3. The transition to charge ordered state takes place at  $V_c^{\text{CE}} \simeq 0.44t$ , that is lower then that one for A- and F- type spin ordering. A smaller value of intersite Coulomb repulsion is needed to introduce the charge ordered state in the state with the lower dimension of ferromagnetic component.

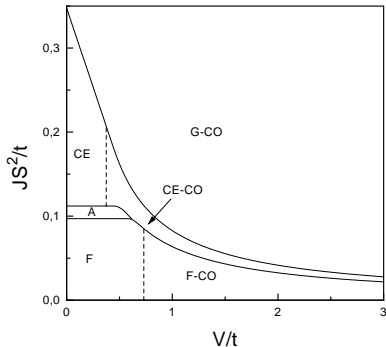


FIG. 5. The phase diagram of the two-orbital model ( $JS^2/t$  vs  $V/t$ ). The dashed lines stand for the second-order boundaries and separate the uniform state from the charge ordered one in the corresponding magnetic phases.

The ground state phase diagram of the two-orbital model is given in Fig.5. The phases with different magnetic structures are separated by the first-order boundaries (solid lines in Fig. 5). The transition from the charge-disordered to the charge-ordered version of the given magnetic structure is continuous, there is no jump in the charge order parameter during the transition which does not change the symmetry of underlying magnetic structure ( the corresponding second-order boundaries are denoted by the dashed lines in Fig.5). At small value of  $V$  with increasing of SE coupling the system goes through four magnetic phases F, A, CE, and G consequently. Due to the additional orbital degree of freedom, unlike to the one orbital model, there exist a finite phase space of A-type spin ordering in the small  $V$  region  $V < V_c^A$ . However, for  $V > V_c^A$ , when the charge ordering is introduced in the A phase, and hence the bandwidth effect is suppressed, CE-CO phase wins and the A-CO phase is never realized in the phase diagram of the present model.

## IV. CONCLUSION

In summary, we have investigated the ground state phase diagram of the one- and two-orbital extended double exchange models within the mean field approximation at half-doping. In the case of the one-orbital model the MF theory predicts the continuous phase transition to the charge ordered state due to the intersite Coulomb interaction  $V$ . In the two-orbital model the character of the transition is changed by the introducing the nonzero critical value of  $V$ . While the transition to charge ordered state with given magnetic structure is continuous, there is jump in of charge order parameter across the phase boundaries between the states with different symmetry of magnetic structure. Depending on the intersite Coulomb interaction  $V$  and superexchange coupling  $J$  different types of spin ordering (F-, A-, G-type) accompanied by the charge ordering may take place in the ground state of the one-orbital model. The presence of orbital degeneracy with the peculiar anisotropic  $e_g$  transfer amplitude introduces the new magnetic state, CE-type spin ordering, in the phase diagram of the two-orbital model. The C-type spin ordering is never achieved within this model due to its instability against the effective "dimerization" and formation of the zig-zag ferromagnetic order. The alternation of the ferromagnetic bonds in  $x/y$  directions leads to the alternation of the hopping amplitude. As a result the bare band is splitted into bonding and anti-bonding states and the "dimerization" gap opens on the Fermi surface at half-doping. The CE-type spin ordered state is accompanied with  $d_{3x^2-r^2}/d_{3y^2-r^2}$  orbital ordering, originated from the topology of the zig-zag structure. The CE-type spin/charge state also wins the CO state with A-type AFM ordering and there exists the phase boundary between the CE spin/charge ordered state and charge disordered (CD) A-type state [see Fig.5]. The experimentally detected competition between A-CD and CE-CO states in the half-doped manganites could indicate that the parameters of the system are close to this phase boundary. Therefore the small change of the bandwidth may drive the system from one to other state. That is also suggested by the huge oxygen isotope effect observed in La-Pr compounds.<sup>19,20</sup> A substitution of  $O^{16}$  by the isotope  $O^{18}$  narrows the carrier bandwidth due to the polaronic effect and as a result the electrostatic energy might overcome the kinetic energy and the charge ordered insulating state might be established.

We would like to point out that there exist other physical factors and ingredients not included in present treatment that may stabilize the particular state and modify the phase diagram (quantum nature of the spins, coupling to the Jan-Teller phonons, and on site Coulomb interaction). As it was recently discussed in Ref. 21 the interorbital on-site Coulomb interaction  $U'$  could be responsible for the experimentally observed charge ordered state. In the CE structure the orbital degeneracy is removed on the sublattice composed by the middle sites

and the low energy state corresponds to the directional orbitals (see Appendix of the present paper). If charge carriers occupy the corner sites there will be a positive contribution from the  $U'$  term to the system energy. While, if only middle site sublattice is occupied this positive contribution disappears since the onsite Coulomb term has the zero matrix element in this case. Therefore,  $U'$  term in CE-type spin ordered state acts as a source of the charge ordering, but in a rather deferent way then the intersite Coulomb repulsion. Since the middle sites are stacked in  $z$ -direction  $U'$  induces experimentally observed  $(\pi, \pi, 0)$  charge ordering instead of the Wigner crystal type CO favored by the intersite Coulomb interaction considered here. Nevertheless, we believe that the main effect of the orbital degeneracy on the interplay of different type of magnetic ordering in charge-ordered state is at least qualitatively captured by the present treatment indicating the crucial importance of the electronic state degeneracy on the phase diagram.

## ACKNOWLEDGMENTS

Financial support by the the INTAS Program, Grants No 97-0963 and No 97-11066, are acknowledged.

## APPENDIX: DIAGONALIZATION IN MOMENTUM SPACE

### 1. Two orbital model

Diagonalization of the Hamiltonian (10) can be done by two subsequent canonical transformation. First, we diagonalize the free part of the Hamiltonian by introducing the new fermionic operators

$$\{d_{\mathbf{k}1} = \tilde{u}_{\mathbf{k}}\bar{d}_{\mathbf{k}1} - \tilde{v}_{\mathbf{k}}\bar{d}_{\mathbf{k}2}, d_{\mathbf{k}2} = -\tilde{v}_{\mathbf{k}}\bar{d}_{\mathbf{k}1} + \tilde{u}_{\mathbf{k}}\bar{d}_{\mathbf{k}2} \quad (\text{A1})$$

with

$$\begin{aligned} H_{\text{el}}^{\text{CE}} = & - \sum_{\mathbf{k}, \alpha, \beta} \left\{ \left[ t_1^{\alpha\beta} \{a_{\mathbf{k}\alpha}^\dagger b_{\mathbf{k}\beta} + \bar{a}_{\mathbf{k}\alpha}^\dagger \bar{b}_{\mathbf{k}\beta}\} + t_2^{\alpha\beta} \{b_{\mathbf{k}\alpha}^\dagger \bar{a}_{\mathbf{k}\beta} + e^{i\mathbf{k}} \bar{b}_{\mathbf{k}\alpha}^\dagger a_{\mathbf{k}\beta}\} + H.c. \right] \right. \\ & \left. - (\mu + \Delta) \{a_{\mathbf{k}\alpha}^\dagger a_{\mathbf{k}\alpha} + \bar{a}_{\mathbf{k}\alpha}^\dagger \bar{a}_{\mathbf{k}\alpha}\} - (\mu - \Delta) \{b_{\mathbf{k}\alpha}^\dagger b_{\mathbf{k}\alpha} - \bar{b}_{\mathbf{k}\alpha}^\dagger \bar{b}_{\mathbf{k}\alpha}\} \right\} \end{aligned} \quad (\text{5})$$

where  $-\pi \leq k \leq \pi$  and the lattice constant is set to be unity ( $a' = 1$  see Fig.4). The above Hamiltonian can be simplified by transforming to new fermion operators  $\{\xi_{\mathbf{k}\alpha}, \bar{\xi}_{\mathbf{k}\alpha}, \eta_{\mathbf{k}\alpha}, \bar{\eta}_{\mathbf{k}\alpha}\}$ ,

$$a_{\mathbf{k}\alpha} = \frac{\xi_{\mathbf{k}\alpha} + \bar{\xi}_{\mathbf{k}\alpha}}{\sqrt{2}}, \quad \bar{a}_{\mathbf{k}\alpha} = e^{i\mathbf{k}/2} \frac{\xi_{\mathbf{k}\alpha} + \bar{\xi}_{\mathbf{k}\alpha}}{\sqrt{2}}. \quad (\text{6})$$

$$\begin{cases} \tilde{u}_{\mathbf{k}} = \frac{|\varepsilon_{\mathbf{k}}^{12}|}{\sqrt{(\varepsilon_{\mathbf{k},1} - \varepsilon_{\mathbf{k},2})(\varepsilon_{\mathbf{k},1} - \varepsilon_{\mathbf{k}}^{11})}} \\ \tilde{v}_{\mathbf{k}} = \frac{\varepsilon_{\mathbf{k}}^{12}}{\sqrt{(\varepsilon_{\mathbf{k},1} - \varepsilon_{\mathbf{k},2})(\varepsilon_{\mathbf{k},1} - \varepsilon_{\mathbf{k}}^{22})}} \\ \varepsilon_{\mathbf{k},1/2} = \frac{1}{2} \left\{ \varepsilon_{\mathbf{k}}^{11} + \varepsilon_{\mathbf{k}}^{22} \pm \sqrt{(\varepsilon_{\mathbf{k}}^{11} - \varepsilon_{\mathbf{k}}^{22})^2 + 4(\varepsilon_{\mathbf{k}}^{12})^2} \right\}. \end{cases} \quad (\text{A2})$$

One finds the effective Hamiltonian of the form

$$\begin{aligned} H_{\text{el}}^{2\text{orb}} = & \sum_{\mathbf{k}, i} \varepsilon_{\mathbf{k}, i} d_{\mathbf{k}i}^\dagger d_{\mathbf{k}i} - \delta \sum_{\mathbf{k}} \text{sgn}(\varepsilon_{\mathbf{k}}^{12}) \\ & \times \left[ d_{\mathbf{k},1}^\dagger d_{\mathbf{k}+\mathbf{Q}2} - d_{\mathbf{k},2}^\dagger d_{\mathbf{k}+\mathbf{Q}1} \right]. \end{aligned} \quad (\text{A3})$$

Further we perform the transformation similar to (6) and introduce the new sets of fermionic operators as

$$\begin{aligned} a_{\mathbf{k}1} = & \bar{u}_{\mathbf{k}1}\bar{d}_{\mathbf{k}1} + \bar{v}_{\mathbf{k}1}\bar{d}_{\mathbf{k}+\mathbf{Q}2}, \quad a_{\mathbf{k}2} = \bar{u}_{\mathbf{k}1}\bar{d}_{\mathbf{k}+\mathbf{Q}2} - \bar{v}_{\mathbf{k}1}\bar{d}_{\mathbf{k}1}, \\ a_{\mathbf{k}3} = & \bar{u}_{\mathbf{k}2}\bar{d}_{\mathbf{k}2} + \bar{v}_{\mathbf{k}2}\bar{d}_{\mathbf{k}+\mathbf{Q}1}, \quad a_{\mathbf{k}4} = \bar{u}_{\mathbf{k}2}\bar{d}_{\mathbf{k}+\mathbf{Q}1} - \bar{v}_{\mathbf{k}2}\bar{d}_{\mathbf{k}2}, \end{aligned}$$

where

$$\begin{aligned} \bar{u}_{\mathbf{k}i} = & \frac{1}{\sqrt{2}} \left[ 1 - \frac{\varepsilon_{\mathbf{k}i}}{E_{\mathbf{k}i}} \right]^{\frac{1}{2}}, \quad \bar{v}_{\mathbf{k}i} = (-1)^i \frac{\text{sgn}(\varepsilon_{\mathbf{k}}^{12})}{\sqrt{2}} \left[ 1 + \frac{\varepsilon_{\mathbf{k}i}}{E_{\mathbf{k}i}} \right]^{\frac{1}{2}} \\ E_{\mathbf{k}i} = & \sqrt{\varepsilon_{\mathbf{k}i}^2 + \Delta^2}, \quad i = 1, 2. \end{aligned}$$

As a result we get the following four band Hamiltonian

$$\begin{aligned} H_{\text{el}}^{2\text{orb}} = & \sum_{\mathbf{k}} \left\{ E_{\mathbf{k}1} [a_{\mathbf{k}1}^\dagger a_{\mathbf{k}1} - a_{\mathbf{k}2}^\dagger a_{\mathbf{k}2}] \right. \\ & \left. + E_{\mathbf{k}2} [a_{\mathbf{k}3}^\dagger a_{\mathbf{k}3} - a_{\mathbf{k}4}^\dagger a_{\mathbf{k}4}] \right\} - \mu \sum_{\mathbf{k}, i=1}^4 a_{\mathbf{k}i}^\dagger a_{\mathbf{k}i}. \end{aligned} \quad (\text{A4})$$

### 2. CE-structure

First, we rewrite the linearized MF Hamiltonian (13) in the momentum space:

The operators  $\{\eta_{\mathbf{k}}, \bar{\eta}_{\mathbf{k}}\}$ , are obtained from  $b_{\mathbf{k}\alpha}, \bar{b}_{\mathbf{k}\alpha}$  by the same transformation as in Eq.(6). One finds the effective Hamiltonian of the form  $H_{\text{el}}^{\text{CE}} = H + \bar{H}$ , where

$$H = - \sum_{\mathbf{k}\alpha\beta} \left\{ t_1^{\alpha\beta} \xi_{\mathbf{k}\alpha}^\dagger \eta_{\mathbf{k}\beta} + t_2^{\alpha\beta} e^{i\mathbf{k}/2} \eta_{\mathbf{k}\alpha}^\dagger \xi_{\mathbf{k}\beta} + H.c. \right\}$$

$$- \sum_{\mathbf{k}\alpha} \left\{ (\mu + \Delta) \xi_{\mathbf{k}\alpha}^\dagger \xi_{\mathbf{k}\alpha} + (\mu - \Delta) \eta_{\mathbf{k}\alpha}^\dagger \eta_{\mathbf{k}\alpha} \right\}, \quad (7)$$

$$\bar{H} = H \left[ \xi(\eta) \rightarrow \bar{\xi}(\bar{\eta}), t_2^{\alpha\beta} \rightarrow -t_2^{\alpha\beta} \right]. \quad (8)$$

Further, we consider only the first part given by (7), generalization of the diagonalization procedure on  $\bar{H}$  is straightforward. With the help of the explicit expression of the hopping amplitude matrix we first transform operators  $\eta_{\mathbf{k}1,2}$  to  $\tilde{\eta}_{\mathbf{k}1,2}$  by the fermionic  $u-v$  transformation with

$$u_{\mathbf{k}} = \frac{1 - e^{ik/2}/2}{\Omega_{\mathbf{k}}}, \quad v_{\mathbf{k}} = \frac{\sqrt{3}e^{ik/2}/2}{\Omega_{\mathbf{k}}}, \quad (9)$$

where  $\Omega_{\mathbf{k}} = \sqrt{2 - \cos \mathbf{k}/2}$ . In terms of the new operators the effective Hamiltonian is written as

$$H = - \sum_{\mathbf{k}} \mathcal{E}_{\mathbf{k}} \left\{ \xi_{\mathbf{k}1}^\dagger \tilde{\eta}_{\mathbf{k}1} + H.c. \right\} - \sum_{\mathbf{k}\alpha} \left\{ (\mu + \Delta) \xi_{\mathbf{k}\alpha}^\dagger \xi_{\mathbf{k}\alpha} + (\mu - \Delta) \tilde{\eta}_{\mathbf{k}\alpha}^\dagger \tilde{\eta}_{\mathbf{k}\alpha} \right\}. \quad (10)$$

where  $\mathcal{E}_{\mathbf{k}} = t\Omega_{\mathbf{k}}$ . The transformed Hamiltonian is already diagonal in the subspace given by the effective orbital index  $\alpha = 2$ . However it mixes the fermionic fields  $\xi_{\mathbf{k}\alpha}$  and  $\eta_{\mathbf{k}\alpha}$  at  $\alpha = 1$ . The hybridization part of the Hamiltonian (10) can be diagonalized following the same rout as in Eqs. (A1,A2). As a result we come to the following diagonal form:

$$H = \sum_{\mathbf{k}} \left\{ \mathcal{E}_{\mathbf{k}} [\beta_{\mathbf{k}1}^\dagger \beta_{\mathbf{k}1} - \beta_{\mathbf{k}2}^\dagger \beta_{\mathbf{k}2}] + \Delta [\beta_{\mathbf{k}3}^\dagger \beta_{\mathbf{k}3} - \beta_{\mathbf{k}4}^\dagger \beta_{\mathbf{k}4}] \right\} - \mu \sum_{\mathbf{k}, i=1}^4 \beta_{\mathbf{k}i}^\dagger \beta_{\mathbf{k}i},$$

$$\bar{H} = H [\beta \rightarrow \bar{\beta}, \mathcal{E} \rightarrow \bar{\mathcal{E}}] \quad (11)$$

where

$$\mathcal{E}_{\mathbf{k}} = \sqrt{\Delta^2 + t^2(2 - \cos k/2)},$$

$$\bar{\mathcal{E}}_{\mathbf{k}} = \sqrt{\Delta^2 + t^2(2 + \cos k/2)}, \quad (12)$$

and  $\beta(\bar{\beta})_{\mathbf{k}3} = \tilde{\eta}(\bar{\eta})_{\mathbf{k}2}$ ,  $\beta(\bar{\beta})_{\mathbf{k}4} = \xi(\bar{\xi})_{\mathbf{k}2}$ , and  $\beta(\bar{\beta})_{\mathbf{k}1,2}$  are given by the linear combination of  $\xi(\bar{\xi})_{\mathbf{k}1}$  and  $\tilde{\eta}(\bar{\eta})_{\mathbf{k}1}$ .

Let us now briefly comment the obtained band structure. It is given by the bonding and antibonding bands  $\mp \mathcal{E}(\bar{\mathcal{E}})_{\mathbf{k}}$  (12) and nonbonding bands  $\pm \Delta$  in between. The nondirectional orbital from the middle sites ( $d_{y^2-z^2}$  and  $d_{x^2-z^2}$  orbitals on  $a$  and  $\bar{a}$  type sites, respectively) is completely decoupled from the other states giving rise to the nonbonding band with energy  $-\Delta$  corresponding to  $\beta(\bar{\beta})_{\mathbf{k}4}$  in Eq.(11). The other nonbonding band with energy  $\Delta$  corresponding to the states  $\beta(\bar{\beta})_{\mathbf{k}3}$  is given by the linear combination of the degenerate orbitals on the corner sites. The state orthogonal to this nonbonding state hybridizes with the directional orbital on the middle sites ( $d_{3x^2-r^2}$  and  $d_{3y^2-r^2}$  orbitals on  $a$  and  $\bar{a}$  type sites, respectively) leading to the bonding and antibonding bands. As follows from the above discussion, the particular geometry of the zig-zag structure not only leads to

the opening of ‘‘dimerization’’-like gap in the spectrum, but also removes the orbital degeneracy on the middle sites. The energy of the directional orbital is lowered due to the hybridization and hence delocalization, while its orthogonal orbital remains local.

- 
- <sup>1</sup> E. O. Wollan, W. C. Koehler, Phys. Rev. B. **100**, 545, (1955).
  - <sup>2</sup> P. Schiffer, A. P. Ramirez, W. Bao, and S.-W. Cheong, Phys. Rev. Lett. **75**, 3336, (1995); S.-W. Cheong and H.Y.Hwang, in: Colossal Magnetoresistance Oxides, ed. Y.Tokura, Gordon & Breach, Monographs in Cond.Matt. Science, (1998); A. P. Ramirez, J. Phys. Cond. Matter **9**, 8171, (1997).
  - <sup>3</sup> C. Zener, Phys. Rev. **82**, 403, (1951); P. W. Anderson, H. Hasegawa, Phys. Rev. **100**, 675, (1955); P. G. de Gennes, Phys. Rev. **118**, 141, (1960).
  - <sup>4</sup> P. G. Radaelli, D. E. Cox, M. Marezio, S-W. Cheong, P. E. Schiffer, and A. P. Ramirez, Phys. Rev. Lett **75**, 4488, (1995).
  - <sup>5</sup> C.H. Chen and S.-W. Cheong, Phys. Rev. Lett. **76**, 4042, (1996).
  - <sup>6</sup> Y.Tomioka, A. Asamitsu, Y. Morimoto, H. Kuwahara, and Y. Tokura, Phys. Rev. Lett. **74**, 5108, (1995).
  - <sup>7</sup> H. Kuwahara, Y. Tomioka, A. Asamitsu, Y. Morimoto, and Y.Tokura, Science **270**, 961, (1995).
  - <sup>8</sup> H. Kawano, R. Kajimoto, H. Yoshizawa, Y. Tomioka, Y. Kuwahara, and Y. Tokura, Phys. Rev. Lett. **78**, 4253, (1997).
  - <sup>9</sup> M. Kubota, H. Yoshizawa, Y. Morimoto, H. Fujioka, K. Hirota, and Y. Endoh, cond-mat/9811192.
  - <sup>10</sup> L. P. Gorkov and V. Z. Kresin, JETP Lett. **67**, 985, (1998).
  - <sup>11</sup> J. van der Brink and D. I. Khomskii, Phys. Rev. Lett. **82**, 1016, (1999).
  - <sup>12</sup> L. Sheng and C. S. Ting, Phys. Rev. B **57**, 5265, (1998).
  - <sup>13</sup> J. D. Lee and B. J. Min, Phys. Rev. B **55**, R14713, (1997).
  - <sup>14</sup> S. Yunoki, J. Hu, A. L. Malvezzi, A. Moreo, N. Furukawa, and E. Dagotto, Phys. Rev. Lett. **80**, 845, (1998).
  - <sup>15</sup> S. K. Mishra, R. Pandit, and S. Satpathy, Phys. Rev. B **56**, 2316, (1997), J. Phys. Cond. Matter **11**, 8561, (1999).
  - <sup>16</sup> S. D. Shen and Z. D. Wang, cond-mat/9906126.
  - <sup>17</sup> S. Yunoki, T. Hotta and E. Dagotto, to appear in Phys. Rev. Lett. (cond-mat/9909254).
  - <sup>18</sup> I.Soloviev and K. Terakura, Phys. Rev. Lett. **83**, 2825, (1999).
  - <sup>19</sup> N. A. Babushkina, L. M. Belova, O. Yu. Gorbenko, A. R. Kaul, A. A. Bosak, V. I. Ozhogin, aand K. I. Kugel, Nature (London) **391**, 159, (1998).
  - <sup>20</sup> A. M. Balagurov, V. Yu. Pomjakushin, D. V. Sheptyakov, V. L. Aksenov, N. A. Babushkina, L. M. Belova, A. N. Taldenkov, A. V. Inyushkin, P. Fischer, M. Gutmann, L. Keller, O. Yu. Gorbenko, and A. R. Kaul, Phys. Rev. B **60**, 383, (1999).
  - <sup>21</sup> J. van der Brink, G.Khaliulin and D.I.Khomskii, Phys. Rev. Lett. **83**, 5118, (1999).